Capillary Flow Properties of Mesh Wicks

J. H. Ambrose* and L. C. Chow†
University of Kentucky, Lexington, Kentucky
and
J. E. Beam‡
Air Force Wright Aeronautical Laboratories, Wright-Patterson Air Force Base, Ohio

The objective of the present investigation is to measure the saturation dependence of the capillary flow properties for multilayer, square-mesh screen wicks. X-ray radiography is used to measure the saturation in the wicks. Results are presented for the capillary pressure vs saturation from steady-state tests. The capillary pressure curves are shown to correlate well when cast in terms of the dimensionless Leverett function. Results of transient wicking rise tests are also presented. The transient saturation distributions are used to calculate the relative permeability of the partially saturated wick structures.

Nomenclature

C = crimping factor
d = filament diameter, m
g = gravitational acceleration, m/s^2
I = radiation intensity
K = full permeability, m^2
K_r = relative permeability
L = thickness of material, m
m = absorbtion coefficient, m^{-1}
N = mesh number, m^{-1}
n = number of layers of mesh
P = liquid pressure, N/m^2
P^* = dimensionless capillary pressure
P_c = capillary pressure, N/m^2
r_p = pore opening, μm
S = saturation
S_i = immobile saturation
t = time, s
U = supercritical flow velocity, m/s
w_S = uncertainty in saturation measurement
x = distance along wick, m
Δt = time between measurements, s
δ = thickness of single layer, m
ϵ = wick porosity
θ = angle of inclination to horizontal
ρ = liquid density, kg/m^3
σ = surface tension, N/m
ϕ = reduced saturation

Introduction

THE flow of fluids in capillary structures has been studied extensively in the past, especially in connection with geological flows. The flow of fluids in porous wick materials has become an important subject because of modern heat transfer applications such as heat pipes and enhanced boiling or condensation surfaces. Detailed modeling of fluid flow in porous materials requires knowledge of the two major flow properties: these are the capillary pressure and the permeability. These two properties are known to depend on the amount of fluid occupying the voids of the porous structure. For flow of the liquid phase, the two properties depend upon the fraction of void space occupied by liquid, which is defined as the saturation.

It is the objective of the current effort to study the saturation dependence of the capillary pressure and permeability for mesh wicks. These materials are commonly utilized in heat pipes because of their uniform structure and ready availability in a wide range of materials and pore sizes. A review of the available literature indicates that much information has been published on the properties of these materials. Extensive data are available concerning the maximum capillary pumping and full permeability (case when fully saturated with single phase) of wick materials. However, relatively little information can be found regarding the saturation dependence of the capillary pressure or the permeability. The accuracy of fluid-flow models for wick structures is limited by this fact—especially if significant saturation gradients or transient saturation distributions occur. Fluid flows in wicks are generally modeled by assuming a fully saturated structure (constant properties). Transient conditions or those involving drying and rewetting of the wick structure are of great interest, and a detailed flow model is necessary for in-depth study of such conditions.

Initial results have been previously presented[1] for the saturation dependence of capillary pressure in a static wicking rise test. Also presented were limited results for mass flow rate and saturation gradient in a wick structure heated at one end. The ratio of superficial velocity to saturation gradient, or "moisture diffusivity," included the lumped saturation dependence of both capillary pressure and permeability. For a given wick, the capillary pressure depends on both saturation and surface tension; whereas permeability depends on saturation alone. It is therefore desirable to separate the two flow properties and study them independently.

Capillary Pressure

The capillary pressure is a function of the saturation and in general it increases with decreasing saturation. It also depends on the wetting properties of the fluid/solid combination. The only fluid/solid combinations of interest to the present study are those that exhibit good wetting, i.e., a near zero contact angle. In addition, the saturation dependence of the capillary pressure is complicated by hysteresis. The functional relation-

Presented as Paper 88-2649 at the AIAA 23rd Thermophysics, Plasmadynamics, and Lasers Conference, San Antonio, TX, June 27-29, 1988; received Sept. 7, 1988; revision received Feb. 27, 1989.

*Research Assistant. Student Member AIAA.
†Professor of Mechanical Engineering. Member AIAA.
‡Technical Area Manager, Nuclear/Thermal Technology Group. Member AIAA.

ship depends upon whether the wetting phase is displacing the nonwetting phase (rising case) or being displaced by it (falling case). There exists in the falling case an irreducible or immobile saturation below which no liquid flow can take place. In this case, called the pendular regime, the discrete portions of the liquid phase can experience mass flow only through evaporation and condensation. This irreducible saturation is evident in the capillary pressure data of Leverett[2] for sands but is absent from the data of Eninger[3] for a metal fiber wick.

For a given fluid/solid combination and a given flow history (rising or falling case), the capillary pressure is a function of saturation alone.[5] The capillary pressure increases with decreasing saturation. As a wetting liquid recedes into the voids of a porous structure, the radii of curvature of the liquid/vapor interfaces will decrease resulting in a greater capillary pressure.

The capillary pressure may be measured under either the static (no flow of liquid) or dynamic conditions (liquid flow due to capillary pressure gradient). Brown[4] has shown the static and dynamic capillary pressure distributions measured in limestone cores to be identical. In the present work, it has been assumed that the relationship is independent of whether the liquid is stationary or moving.

Relative Permeability

When two or more phases are present in a porous material, the permeability becomes less than for a single phase. In the case of a wetting and nonwetting phase, the wetting phase must flow around the voids occupied by the nonwetting phase. The decrease in permeability is a direct result of the increased tortuosity of the flow paths. In such a case, the relative permeability is used. The relative permeability is defined by assuming that the flow of each phase through the porous material is governed by Darcy's law with a different permeability to each phase. The relative permeability so defined has been shown[5] in numerous experiments to depend on saturation alone. (Actually, a weak dependence on overpressure is exhibited, but this is not applicable to the present case where no overpressure exists.) The relative permeability (as a function of saturation) is much more difficult to measure than the full permeability. However, extensive measurements have been conducted for geological materials. In general, the relative permeability of a porous material to a particular phase increases monotonically with the saturation of the phase.

Other Related Work

Extensive modeling of heat transfer and fluid flow in partially saturated packed beds of sand, including the effect of saturation gradients on capillary pressure and relative permeabilities, has been carried out by Udell[6,7] and Fitch and Udell.[8] Available data for the sand/water system were utilized to model these effects. In particular, the researchers have successfully used a correlation for dimensionless capillary pressure based on the data of Leverett[2] and the following relative permeability expressions for the liquid and vapor phases, respectively,

$$K_{rl} = \phi^3$$

$$K_{rv} = (1 + \phi^3)$$

where the reduced saturation is defined by

$$\phi = \frac{(S - S_i)}{(1 - S_i)}$$

The third power saturation dependence of the relative permeability to the liquid phase has been shown to be in good agreement with experimental data for granular porous media.[5]

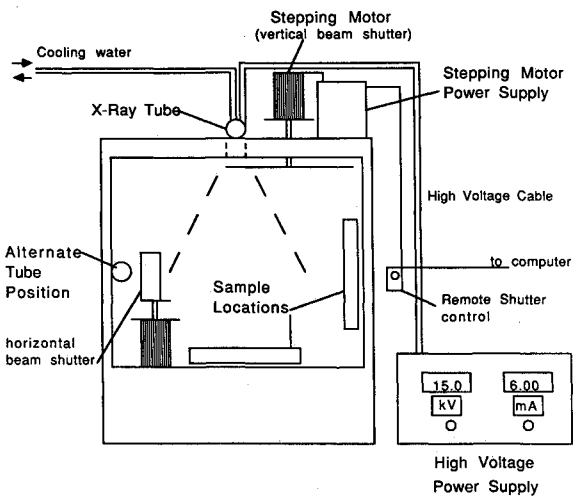

Fig. 1 Schematic of x-ray saturation measurement.

Description of Experiment

An experimental study of the saturation dependence of the capillary pressure and permeability in mesh wicks has been conducted. Both transient and steady-state wicking tests were performed. The key feature of these experiments is the use of x-ray radiography for the measurement of saturation. The experimental setup is shown in Fig. 1.

The wicks were radiographed using a 30 kV, 6.7 mA Kevex tungsten target x-ray source (tube voltage set at 15 kV). The saturation distributions were determined using a special digitizing system consisting of a computer controlled x-y film positioner and an X-Rite 301RS black-and-white photodensitometer. Saturation measurements were taken on a 2.54 mm by 2.54 mm grid and then averaged in the direction perpendicular to the pressure gradient.

Because the pressure distribution at equilibrium is hydrostatic, the capillary pressure is a linear function of distance above the free surface. When a radiograph of the wick is analyzed, it yields the saturation as a function of position. Thus each radiograph yields an entire capillary pressure/saturtion curve from a single test.

The wick materials used were all square-mesh, synthetic fabrics obtained from Tetko Inc. Their relevant properties are given in Table 1. The wick structures were formed by pressing several layers of material tightly between two flat beryllium plates. This was required to maintain the wicks in a planar geometry and insure good contact between layer of wick material. Two points need to be addressed concerning the geometry of the wick structures so formed: clamping pressure and boundary influence.

Clamping Pressure

To provide a uniform structure, each multilayer wick was clamped with approximately 0.15–0.35 N/m^2 pressure over the approximately 77 cm^2 area. The pressure exerted on the layers was enough to press them tightly together but not enough to cause significant deformation of the fibers as determined from subsequent examination. The beryllium plates are extremely rigid and were clamped in several locations to insure a uniform pressure. In previous attempts spacers were used to provide a uniform thickness of the clamped wick. The obvious choice for this spacing was the total thickness of the clamped layers. However, when the space between the plates was made equal in thickness to n times δ, it was found that the wick layers were still somewhat loose and pockets of gas would be trapped in the open spaces. This occurs because the layers tend to intermesh and occupy less space. When the layers were clamped together, a much more uniform structure was obtained as evidenced by the equilibrium distributions of liquid and gas in the structures.

Influence of the Wall

The present wick geometry (bounded on both sides) is different than that in a heat pipe, where the wick is bounded on

Table 1 Wick material properties

Material type	N, cm^{-1}	d, μm	δ m^2	K, $\times 10^{-10}$, m^2	ϵ	r_p, μm	n
Polypropylene							
5-280	22.8	160	320	7.88	0.70	280	5
Polyesters							
HC7-200	33.3	100	165	4.18	0.73	200	12
HC7-85	80.0	40	67	0.74	0.73	85	25[a]
HC7-51	119.0	33	65	0.26	0.68	51	25[a]

[a]Fifteen layers of HC7-85 and HC7-51 were used in the transient tests.

only one side by a solid surface. The other side is usually open to provide for vapor escape. However, it is felt that the influence of the wall on the flow properties can be neglected in the case of a multilayer wick structure with uniformly clamped layers. Most wick structures are constructed of multiple layers in order to provide sufficient flow area. The influence of the boundary on flow is known to be confined to a very small region near the wall. In Darcy flow, the momentum boundary layer is of the order of $\sqrt{K/\epsilon}$.[9] For the wicks used in the present experiment, this value is of the order of 10 μm or less (less than 0.1% of the wick thickness). In addition, the effective pore size is not thought to be significantly changed by the presence of the additional wall. The pumping is controlled by the smallest voids in the mesh material in which two-phase interfaces are present. The size of such voids depends mainly on the filament diameter and spacing of the filaments. It is commonly assumed that reductions in saturation in a mesh wick occur by a uniform recession of the liquid/vapor interface into the first layer of the wick. Saturation measurements made by the authors show that, in the actual wick, the interfaces are irregular and the nonwetting phase penetrates deep into the wick structure at various locations. Thus, the nonwetting phase is more evenly distributed over the cross section of the wick. The mesh structure is not perfectly uniform (at the micron scale), and liquid recessions occurs more readily at some locations than others. For this reason the macroscopically observed wick properties depend much more on the wick material than on the boundary conditions or number of layers. This is similar to the case of a uniformly random porous packing of sand in a container. If the walls of the container do not alter the packing geometry, then they have little if any effect on the capillary properties of the bulk material of the bed.

Steady-State Tests

The steady-state wicking apparatus is shown in Fig. 2. A closed system was utilized to minimize the effects of evaporation of the liquid on the final equilibrium distribution. The design is similar to that used by Shibayama and Morooka[10] with the addition of the saturation measurement. A metal marker was used to show, on the radiograph, the location of the free liquid interface in the glass tube. For each test, the wick was cleaned in acetone, rinsed with methanol, filtered through a 0.2 μm filter, and dried with filtered air. It was then assembled into the holder, and the beryllium plates were sealed in place with silicone sealant.

The nonwetting phase for the steady-state tests was a mixture of air and methanol vapor. The presence of air mainly affects the evaporation rate and the phase-change temperature. An equilibrium concentration of vapor is reached in the apparatus within a short period of time after which evaporation becomes negligible. The capillary pressure is not significantly different for the air/liquid system compared with the vapor/liquid system.

The steady-state tests were to be performed with Freon-113 because of its superior x-ray attenuation property. However, Freon-113 was found to be incompatible with the sealant; therefore doped methanol was used in its place. The methanol was doped with a small amount (0.0375 g/ml) of potassium iodide to increase x-ray absorption. Rise tests were conducted in capillary tubes to verify that the small amount of impurity has a negligible effect on surface tension and contact angle.

A radiograph was taken of the assembly with a dry wick. Kodak Type M industrial radiography film was used for the steady-state tests. Liquid was added to the glass tube. More liquid was added as necessary to maintain the liquid level in the glass tube. Equilibrium was assumed to have been reached when the liquid level in the tube stopped falling, and another radiograph was taken to determine the rising saturation distribution. The duration of the steady-state test was of the order of 1 h.

Transient Tests

Transient wicking tests were conducted with an open system. Because of the much shorter duration of these tests (of the order of 1 min), evaporation is assumed to be negligible compared to the liquid-flow rates. The wick layers were clamped between the two beryllium plates with the sides open to the atmosphere. Each test consisted of placing the wick in contact with a constant head reservoir of liquid at time $t = 0$. For the HC7-51 material, the wick was in a vertical position. For the other materials, the wick was inclined at a small angle to the horizontal to increase the wicking distance. Freon-113 was used in the transient tests because of its good x-ray attenuation.

Each radiograph taken during the transient yields the saturation as a function of position. The saturation distributions were measured at intervals of 15–45 s with a 1 s exposure time.

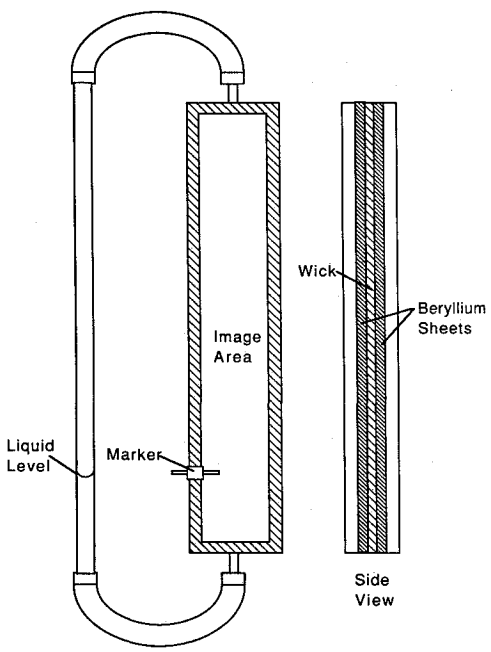

Fig. 2 Schematic of steady-state wicking apparatus.

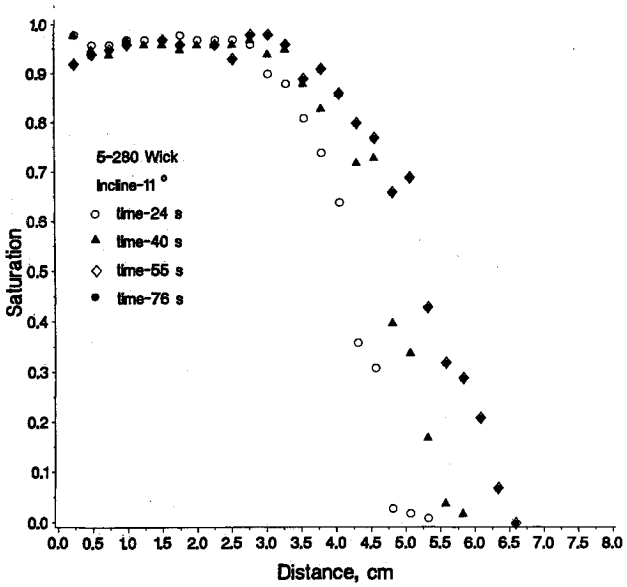

Fig. 3 Transient saturation curves for 5-280 wick.

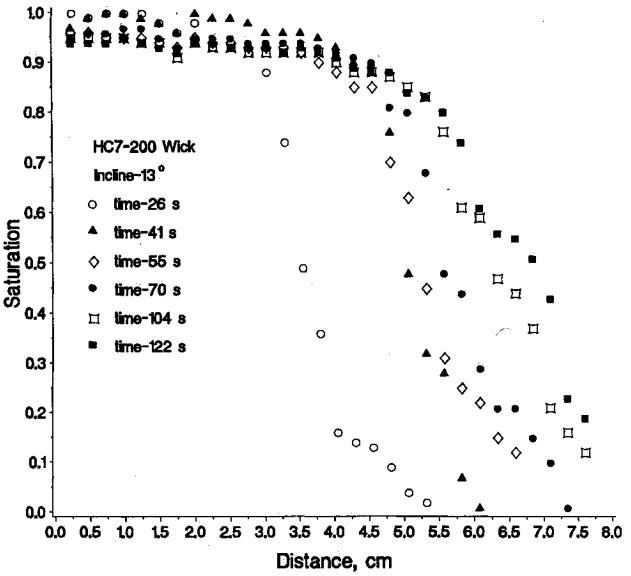

Fig. 4 Transient saturation curves for HC7-200 wick.

The short exposure times were made possible through use of high-speed, Kodak direct-exposure x-ray film. The flow in this case is a moving front characteristic of that which occurs when a previously dry wick structure is rewetted with liquid. After equilibrium has been established, the pressure gradient is hydrostatic, and the usual curve of static capillary pressure vs saturation may be obtained.

Transient saturation distributions for the four wick materials in Table 1 are shown in Figs. 3–6. The angle of inclination to the horizontal is indicated for each material. The time values correspond to seconds elapsed since filling and distances are measured along the wick from the free liquid surface.

The transient saturation curves of the finer mesh wicks (HC7-51, HC7-85) are smoother than those of the coarser wicks (5-280, HC7-200). These wicks behave more uniformly because of the greater number of pores (many layers, small pore size). Because of the lower permeability of the finer mesh, the flow velocity is much less. This increased the distance between the wicking front in the successive images and allowed better resolution. For the 5-280 wick, the wicking front quickly approaches its maximum height. In the present experiment, the successive images could not be attained quickly enough to show this initial surge.

The present results are in qualitative agreement with measurements of Beam[11] for copper screen wicks. Both show a rapid rise to near equilibrium followed by a very slow creeping flow. It appears that the shape of the saturation profiles do not change markedly with time. All show a sharp drop in saturation corresponding to the moving front. A much larger saturation gradient is required to sustain the flow at this front than in the fully wetted portion of the wick.

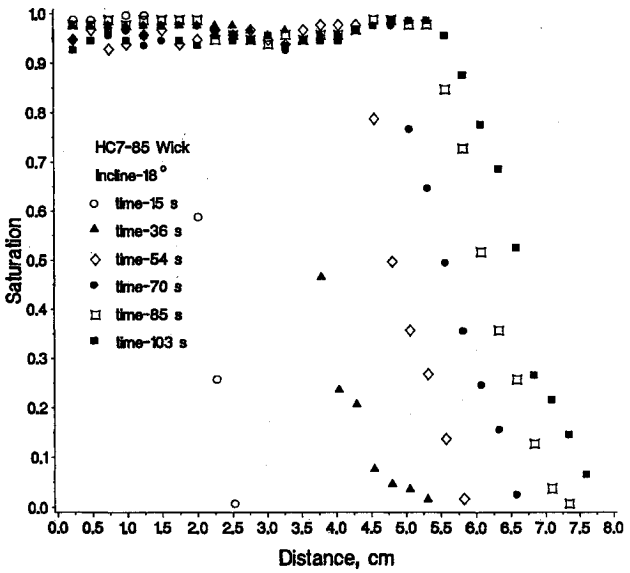

Fig. 5 Transient saturation curves for HC7-85 wick.

Analysis and Discussion of Results

Dimensionless Capillary Pressure

The steady-state data for the four different wick materials of Table 1 are shown in Fig. 7. These values have been nondimensionalized using the Leverett function[2]

$$P^* = (P_c/\sigma)\sqrt{K/\epsilon} \tag{1}$$

The permeability was calculated based on the Blake-Kozeny equation[12]

$$K = \frac{\epsilon^3 d^3}{122(1-\epsilon)^2} \tag{2}$$

The porosity is based on the equation of Marcus[12]

$$\epsilon = 1 - (\pi CNd/4) \tag{3}$$

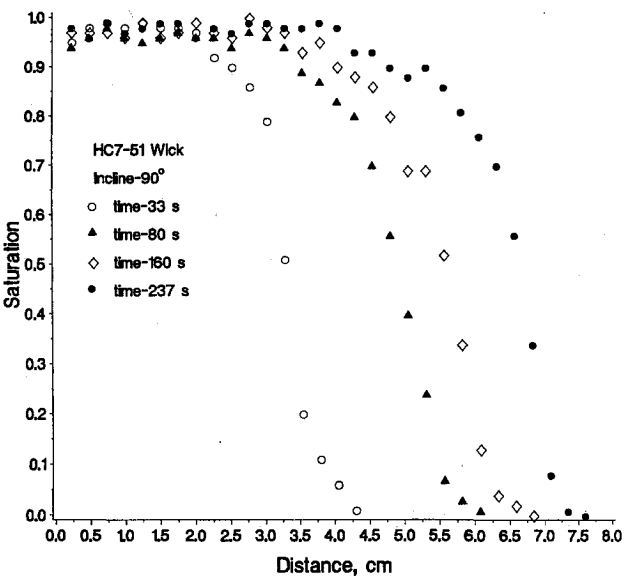

Fig. 6 Transient saturation curves for HC7-51 wick.

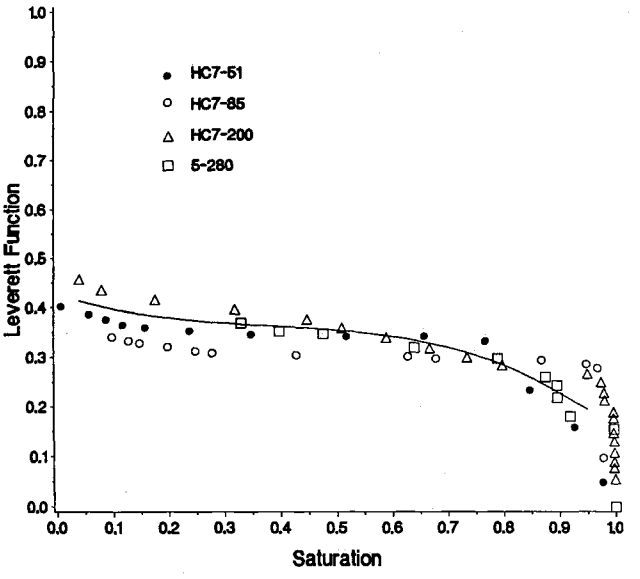

Fig. 7 Dimensionless capillary pressure curves.

where N is the mesh number and the "crimping factor" C is taken to be 1.05. This value is suggested by Chi[12] for multilayer wicks where the layers are pressed tightly together. Values of full permeability and porosity calculated using Eqs. 2 and 3 are given in Table 1.

The capillary pressure curve (Fig. 7) indicates that the largest capillary pressure difference is attained with a relatively small reduction in S. The P_c increases as S decreases to about 0.9, then levels off, with another small increase near $S=0$. This reflects a rather steep drop in saturation near the top of the column of liquid which is identified as the "wicking front."

Further data for a metal felt wick[3] and for clean sands[2] are compared with the present data in Fig. 8. The good agreement for saturations between 0.1 and 0.9 is surprising given both the differences in geometry of the porous materials and the additional uncertainty introduced by using Eqs. (2) and (3). The good correlation of the capillary pressure data means that the relationship can be extended with confidence to other mesh materials without further measurements provided of course that the contact angle is near zero and the porosity and permeability are known. A curve fit of the present data for saturations less than 0.9 is also shown in Fig. 7. This curve fit was used in the calculation of relative permeabilities in the following section.

Calculation of Relative Permeability

Data for transient saturation distributions given in Figs. 3–6 were used to calculate relative permeabilities. In order to obtain the relative permeability from the data, Darcy's law is used.

$$U(x) = -\frac{KK_r}{\mu}\frac{dP}{dx} \tag{4}$$

Here x is measured along the wick in the direction of the flow with $x=0$ at the reservoir. In the transient case, P is not known directly; therefore it is written in terms of position

$$P = P_0 - (P_c - \rho g x \sin\theta) \tag{5}$$

Here P_0 is the liquid pressure (atmospheric) at the level of the reservoir. This yields the liquid pressure gradient in terms of the capillary pressure function, the saturation gradient, and the angle of inclination:

$$\frac{dP}{dx} = \rho g \sin\theta - \frac{dP_c}{dS}\frac{dS}{dx} \tag{6}$$

The function dP_c/dS is taken to be a property of the wick structure and is obtained from the equilibrium data (curve fit in Fig. 7). The saturation gradient and flow velocity are obtained from the transient saturation distributions as follows. Let $S_1(x)$ and $S_2(x)$ represent the saturation distributions with distance at times $t=t_1$ and $t=t_2$, respectively, where $t_2 - t_1 = \Delta t$. The saturation gradient used in the calculation of relative permeability is

$$\left.\frac{dS}{dx}\right|_{x_0} = \frac{1}{2}\left(\left.\frac{dS_2}{dx}\right|_{x_0} + \left.\frac{dS_1}{dx}\right|_{x_0}\right) \tag{7}$$

The flow velocity is given by

$$U(x_0) = \left[\int_{x_0}^{x_\infty} S_2(x)dx - \int_{x_0}^{x_\infty} S_1(x)dx\right] \Big/ (\Delta t/\epsilon) \tag{8}$$

where x_∞ is the position at which $S=0$, and the saturation of interest is $S(x_0) = [S_2(x_0) + S_1(x_0)]/2$. Reynolds numbers based on the velocity calculated from the data and the pore opening are of the order of 0.1. Darcy's law is therefore valid in this regime.

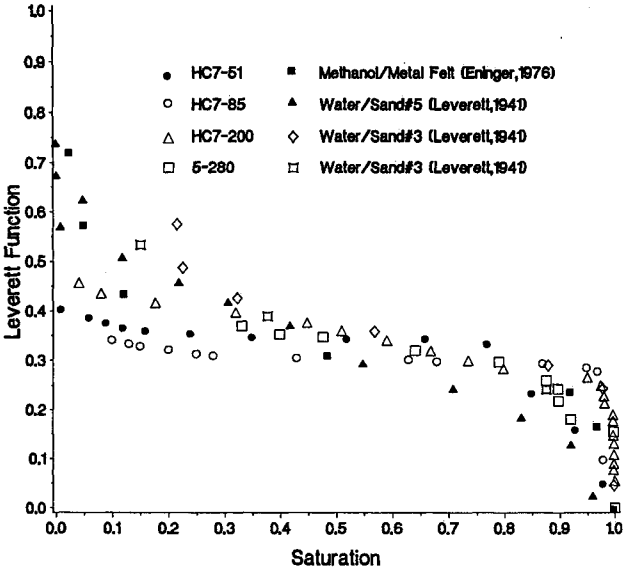

Fig. 8 Comparison of capillary pressure curves.

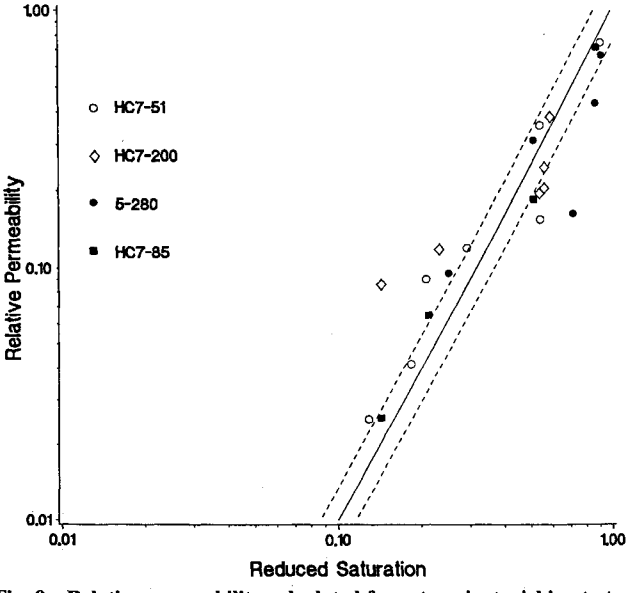

Fig. 9 Relative permeability calculated from transient wicking tests.

The relative permeability is given in Fig. 9 as a function of reduced saturation for the four different meshes. The solid line represents reduced saturation to the second power. The dotted lines show the deviation of ± 30% from this line. The significant amount of scatter in the data is to be expected because of the uncertainty associated with both the raw saturation data and the calculation procedure. An additional uncertainty is introduced when calculating gradients from the raw saturation data. For a detailed discussion, see the Appendix.

The relative permeability values calculated for the HC7-51 and HC7-85 wicks show less scatter than those for the coarser meshes. This is expected because of the nature of the transient wicking curves discussed earlier. The curves for the finer meshes were smoother and farther apart allowing a more accurate determination of the relative permeability. Because these results were considered to be more accurate, they were weighted accordingly when the exponent was estimated. The relative permeability data follow roughly the same trend as those for geological materials.

Conclusions

The equilibrium data in Figs. 7 and 8 show the validity of the dimensionless scaling proposed by Leverett. The data for different fluids and different types of wick structures correlate well. This supports the present assumptions concerning the multilayer wick structures used in the experiments and allows a determination of the capillary pressure/saturation relationship based on well-established properties of the wick material and fluid.

The transient wicking data agree qualitatively with earlier results,[11] which show a rapid rise to near equilibrium height followed by a slow climb toward final equilibrium. Relative permeability values have been obtained from the transient wicking rise curves. These values show the expected monotonically increasing trend. They are satisfactorily described by reduced saturation raised to the power two.

The flow parameters of capillary pressure and relative permeability in mesh wicks depend heavily on the liquid saturation. These relationships have been measured for a range of mesh sizes. They have been shown to be similar to those found for packed granular materials such as sand. Such relationships have not previously been generally utilized in the modeling of liquid flow in wick structures. The present results will allow a more detailed model of the liquid flow in mesh wick structures and contribute to the overall understanding of the transient operation of such devices as heat pipes and wicked heat transfer surfaces, including such phenomena as dryout and rewetting.

Appendix: Uncertainty in Saturation Measurement

In any experiment, the uncertainty of measurements is important in determining the value of the results. In the present work, the most crucial value measured was the saturation. This value involved a complex measurement procedure, and there are two important areas of uncertainty.

Constant Wavelength Assumption

The saturation is determined by comparison of optical densities taken from x-rays. X-rays were taken of wicks which were deemed to be completely dry or fully saturated. The saturation was calculated assuming a constant attenuation coefficient. Bouguer's law relating incident and transmitted radiation intensities is given as

$$I/I_0 = \exp(-mL) \tag{A1}$$

where m is the absorption coefficient and L the thickness of material penetrated. In this relation m is considered constant. It actually depends on wavelength; therefore this relation holds only for monochromatic radiation. The radiation from an x-ray tube is white radiation and as such, the energy distribution of the beam will change upon passing through a material. The weaker, longer wavelengths will be absorbed much more than the shorter ones. The value of using the constant attenuation coefficient or constant wavelength assumption can be assessed by plotting the logarithm of the intensity ratio vs thickness of material penetrated. In the present investigation, this was accomplished by making a wedge-shaped vessel using two beryllium plates. The plates touched each other at one end and separated to a spacing of about 0.6 cm at the other end, about 28 cm away. The void in this vessel was filled with freon working fluid and x-ray radiographs were taken. The thickness of fluid penetrated was thus linear, and the plot of optical density vs thickness is shown in Fig. A1. It should be noted in this plot that the behavior can be approximated as linear provided that the thickness range is not large. For thicknesses of 0–1 mm, the maximum deviation from linear behavior is about 10%. This means that the saturation measurements in this study were subject to an additional uncertainty of up to 10%. This uncertainty decreases as the limiting saturations of zero and one are approached.

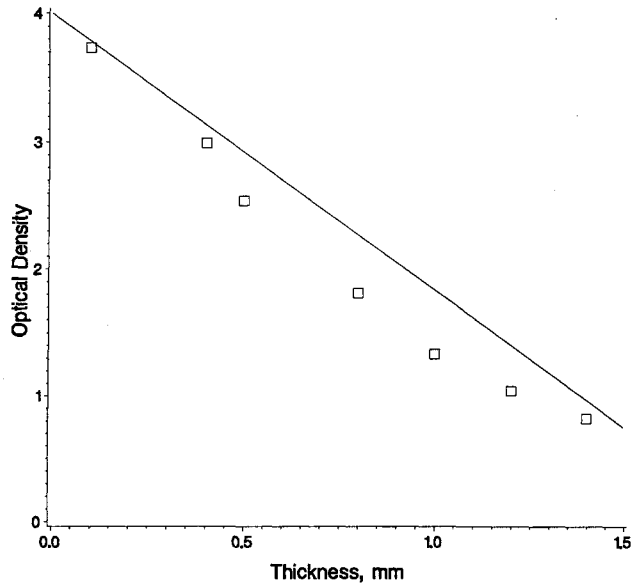

Fig. A1 Optical density vs liquid layer thickness.

Table A1 Uncertainty of S

S	0.1	0.2	0.4	0.6	0.8	1.0
W_S	0.27	0.13	0.06	0.04	0.03	0.028

Uncertainty of Saturation Measurement

As stated above, each saturation value was calculated based on three optical density readings. The uncertainty of the final saturation value depends on both the magnitude of the three readings and their individual uncertainty, which is given for the photodensitometer as $\pm 0.02\ D$. Based on these values, the percentage of overall uncertainty W_S in the saturation value can be approximated by $0.028\sqrt{1 + 1/S^2 - 1/S}$).[13] This uncertainty is tabulated in Table A1.

Based on the two preceding uncertainties, the overall uncertainty in S is approximately 20%, but becomes larger for saturations less than 10%.

The capillary pressure itself is based on measurement of distance on the radiographs and is subject to an uncertainty of only a few percent.

Uncertainty of Relative Permeability Calculation

The relative permeability values are given by

$$K_r = \mu U/[K(dP_c/dx)(dS/dx)] \tag{A2}$$

The term which introduces the greatest uncertainty in this equation is the saturation gradient. This was obtained by first fitting the saturation data with a second order polynomial over the region of interest and then calculating the derivative of the polynomial. If the polynomial in x is given by

$$S = \beta_0 + \beta_1 x + \beta_2 x^2 \quad \text{(A3)}$$

then the variance of the slope is given by

$$\text{var}\,(dS/dx) = \text{var}\,(\beta_1) + 4x^2\,\text{var}\,(\beta_2) + 2x\,\text{cov}\,(\beta_1\beta_2) \quad \text{(A4)}$$

The variance data was calculated for the various quantities and for the multiple curves. From this the standard deviation of the derivative term was found to be 25-30%. Based on this and the uncertainty of measurement associated with S itself, the uncertainty in the relative permeability calculation is estimated to be as large as 50% for the lower saturation range. This large uncertainty is reflected by the scatter in the relative permeability data.

Acknowledgments

The work described in this paper was sponsored by the Aero Propulsion Laboratory, U. S. Air Force Wright Aeronautical Laboratories, Aeronautical Systems Division, Wright-Patterson AFB, Ohio. The experiments were performed at the University of Kentucky at Lexington.

References

[1]Ambrose, J. H., Chow, L. C., and Beam, J. E., "Measurement of Liquid Flow in Heat Pipe Wicks," AIAA Paper 87-1647, 1987.

[2]Leverett, M. C., "Capillary Behavior in Porous Solids," *Transactions of the AIME*, Vol. 142, 1941, pp. 152-169.

[3]Eninger, J. E., "Capillary Flow through Heat-Pipe Wicks," *Progress in Astronautics and Aeronautics: Radiative Transfer and Thermal Control*, Vol. 49, edited by A. Smith, AIAA, New York, 1976, pp. 435-459.

[4]Brown, H. W., "Capillary Pressure Investigations," *Transactions of the AIME*, Vol. 192, 1951, pp. 67-74.

[5]Scheidegger, A. E., *The Physics of Flow Through Porous Media*, Macmillan, New York, 1957.

[6]Udell, K. S., "Heat Transfer in Porous Media Heated from Above with Evaporation, Condensation and Capillary Effects," *Journal of Heat Transfer*, Vol. 105, No. 3, 1983, pp. 485-492.

[7]Udell, K.S., "Heat Transfer in Porous Media Considering Phase Change and Capillary—the Heat Pipe Effect," *International Journal of Heat and Mass Transfer*, Vol. 28, No. 2, 1985, pp. 485-495.

[8]Fitch, J. S. and Udell, K. S., "Limits of Multiphase Heat and Mass Transfer in Porous Media," American Society of Mechanical Engineers, Paper 86-HT-33, 1986.

[9]Vafai, K. and Tien, C. L., "Boundary and Inertia Effects on Flow and Heat Transfer in Porous Media," *International Journal of Heat and Mass Transfer*, Vol. 24, 1981, pp. 195-203.

[10]Shibayama, S. and Morooka, S., "Study on a Heat Pipe," *International Journal of Heat and Mass Transfer*, Vol. 23, 1980, pp. 1003-1013.

[11]Beam, J. E., "Unsteady Heat Transfer in Heat Pipes," Ph.D. Dissertation, School of Engineering, University of Dayton, Dayton, OH, 1985.

[12]Chi, S. W., *Heat Pipe Theory and Practice*, McGraw-Hill, New York, 1976.

[13]Holman, J. P., *Experimental Methods for Engineers*, McGraw-Hill, New York, 1978.